PHOTONICS Research

Tunable broadband two-point-coupled ultra-high-Q visible and near-infrared photonic integrated resonators

Kaikai Liu,[1] Nitesh Chauhan,[1] Meiting Song,[1] Mark W. Harrington,[1] Karl D. Nelson,[2] and Daniel J. Blumenthal[1,*]

[1]Department of Electrical and Computer Engineering, University of California Santa Barbara, Santa Barbara, California 93106, USA
[2]Honeywell Aerospace, Plymouth, Minnesota 55441, USA
*Corresponding author: danb@ucsb.edu

Received 29 April 2024; revised 29 June 2024; accepted 1 July 2024; posted 3 July 2024 (Doc. ID 528398); published 19 August 2024

Ultra-high-quality-factor (Q) resonators are a critical component for visible to near-infrared (NIR) applications, including quantum sensing and computation, atomic timekeeping and navigation, precision metrology, microwave photonics, and fiber optic sensing and communications. Implementing such resonators in an ultra-low-loss CMOS foundry compatible photonic integration platform can enable the transitioning of critical components from the lab- to the chip-scale, such as ultra-low-linewidth lasers, optical reference cavities, scanning spectroscopy, and precision filtering. The optimal operation of these resonators must preserve the ultra-low losses and simultaneously support the desired variations in coupling over a wide range of visible and NIR wavelengths as well as provide tolerance to fabrication imperfections. We report a significant advancement in high-performance integrated resonators based on a two-point-coupling design that achieves critical coupling simultaneously at multiple wavelengths across wide wavebands and tuning of the coupling condition at any wavelength, from under-, through critically, to over-coupled. We demonstrate critical coupling at 698 nm and 780 nm in one visible-wavelength resonator and critical coupling over a wavelength range from 1550 nm to 1630 nm in a 340-million intrinsic Q 10-meter-coil waveguide resonator. Using the 340-million intrinsic Q coil resonator, we demonstrate laser stabilization that achieves six orders of magnitude reduction in the semiconductor laser frequency noise. We also report that this design can be used as a characterization technique to measure the intrinsic waveguide losses from 1300 nm to 1650 nm, resolving hydrogen-related absorption peaks at 1380 nm and 1520 nm in the resonator, giving insight to further reduce waveguide loss. The CMOS foundry compatibility of this resonator design will provide a path towards scalable system-on-chip integration for high-performance precision experiments and applications, improving reliability, and reducing size and cost.

https://doi.org/10.1364/PRJ.528398

1. INTRODUCTION

Ultra-high-quality (Q)-factor resonators are a critical technology for generating spectrally pure light, providing optical frequency references, and other functions that benefit a wide array of precision scientific applications, including quantum sensing and computing, coherent communications [1–3], precision metrology [4], optical atomic clocks [5], and low-noise microwave and millimeter-wave generation [6–8]. There have been advancements in integrating these resonators fabricated in the CMOS foundry compatible ultra-low-loss silicon nitride waveguide platform [9] with a significant reduction in propagation loss and increased Q at the near-infrared (NIR) [10–13] and visible wavelengths [14], as well as in realizing ultra-narrow-linewidth high-power lasers [13,15–17] and integrated optical stabilization cavities [18,19] for applications such as atomic, optical, and molecular (AMO) experiments [20] and ultra-low-phase-noise microwave and mmWave generation [7,8]. Enabling these resonators to be designed for optimal operation in a wide range of wavelengths, across the visible to NIR, and integration with other components at the wafer-scale will transform precision table-top systems to chip-scale [21,22].

Waveguide propagation loss and resonator Q are critical for the application performance and have made significant progress [10,11,13,14]. However, other key considerations remain to be addressed, including realizing the desired resonator coupling regime, i.e., the degree of coupling: under-, over-, or critically coupled [23]. Critical coupling is desirable when the resonance is at its minimum and the extinction ratio is at its maximum for stimulated Brillouin scattering lasers (SBLs) to achieve

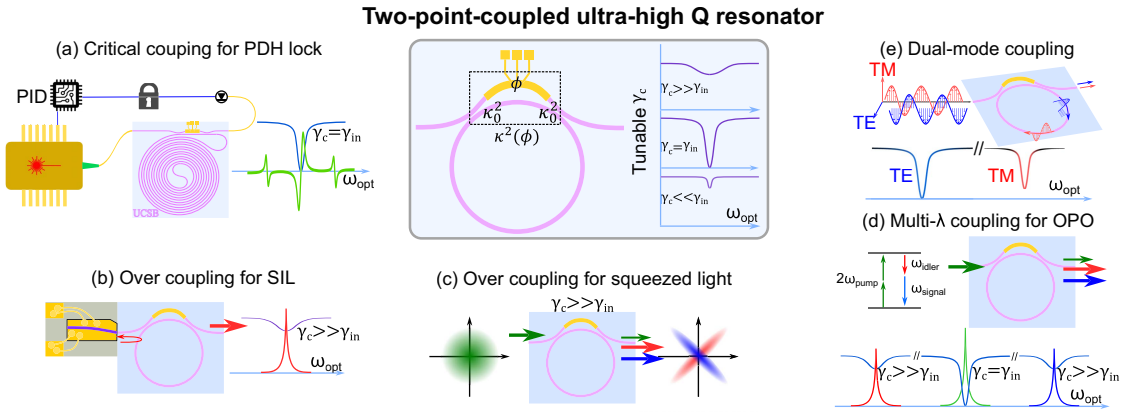

Fig. 1. Illustration of the working principles of two-point coupling for waveguide resonators shows the tunable bus-resonator coupling expressed by $\kappa^2(\phi) = 4\kappa_0^2(1-\kappa_0^2)\cos^2(\phi/2)$, and the tunable bus-resonator coupling rate expressed by $\gamma_c = c\kappa^2(\phi)/n_g L$. Panels (a) to (e) show two-point-coupled ultra-high Q resonators for various applications, such as (a) critically-coupled ultra-high-Q reference resonators for PDH lock and laser stabilization, (b) over-coupled resonators for increased feedback and output power in self-injection locked lasers, (c) squeezed light generation in over-coupled resonators, (d) multi-wavelength coupling design for efficient OPO processes, and (e) dual-mode (TE-TM) coupling. TE, transverse electric. TM, transverse magnetic. SIL, self-injection locked laser. PDH, Pound–Drever–Hall. OPO, optical parametric oscillation.

a low optical threshold, high Brillouin conversion efficiency, high output power, and narrow fundamental linewidth [16,17,24–26]. The ability to achieve critical coupling at a particular wavelength is also important for narrow-linewidth visible and NIR emission SBLs [27]. As shown in Fig. 1, laser stabilization with waveguide resonators leverages long coil waveguides to increase the mode volume to lower the thermo-refractive noise (TRN) floor [19,28,29]. Meter-scale coil silicon nitride waveguide resonators with Q greater than 100 million are capable of narrowing the integral laser linewidth to 36 Hz and stabilizing the carrier to an Allan deviation of 1.8×10^{-13} at 10 ms [19]. Such resonators require operation at the critical coupling point at the desired stabilized laser wavelength to maximize the signal-to-noise ratio (SNR) in the laser frequency noise discrimination and noise suppression processes [Fig. 1(a)] [30]. Over-coupled designs in self-injection locked lasers (SILs) can increase the output power in the through port by reducing the resonator power dissipation and suppressing unwanted nonlinear parametric processes [Fig. 1(b)] [31,32]. Squeezed light generation requires over-coupling in the squeezing mode, whereas the pump modes are critically coupled [Fig. 1(c)] [33,34]. Applications such as optical parametric oscillation (OPO) processes benefit from critical coupling at two or more wavelengths simultaneously [Fig. 1(d)] [35,36]. Other applications require resonators to be critically coupled at both fundamental and second harmonic wavelengths simultaneously [37,38], or both transverse-electric (TE) and transverse-magnetic (TM) modes [Fig. 1(e)] [39], where such a dual-wavelength or dual-mode coupling design can be particularly challenging [37]. Integrated large optical mode volume coil resonators have been used to demonstrate laser frequency referencing for trapped ion qubit and clock operation applications [20], and to generate record-low phase noise microwaves and mmWave [7,8]. There is strong motivation to integrate these ultra-high-Q resonators and provide laser and systems-on-chip solutions. Additionally, integrated bus-coupled resonators, particularly at shorter visible wavelengths, are susceptible to fabrication imperfections and variations in the bus-to-resonator coupling.

The coupling wavelength and coupling regime using bulk-optic resonator designs have been addressed using whispering-gallery-mode (WGM) resonators that employ a fiber taper with a coupling strength tuned by adjusting the fiber taper position to the resonator [24,25,40]. Integrated versions have utilized a silicon nitride bus waveguide fabricated with an etched silica WGM resonator to improve robustness, but without the capability to tune the resonator coupling [25]. Post-processing trimming in silicon photonics can correct the microring resonant wavelength but produces relatively small changes in either the bus-ring resonator coupling or resonance extinction ratio [41,42]. *In-situ* resonator coupling tuning has been demonstrated in silicon microring resonators using thermal gradient tuning [43,44] and an unbalanced Mach–Zehnder interferometer (MZI) two-point-coupler [45,46]. However, tunable resonator coupling has not been demonstrated in ultra-high-Q waveguide resonators in the regime of ~100 million and larger [10,13,47]. Recently, virtual critical coupling and efficient cavity energy loading in a silicon nitride ring resonator are demonstrated by adding an exponentially growing pulse shape to the continuous-wave (CW) pump laser [48]. However, direct engineering of the resonator coupling is preferable and can be suitable for a broader range of applications.

In this paper, we report a major advancement in ultra-high-Q integrated silicon nitride waveguide resonators using a thermally actuated tunable two-point-coupler design. We demonstrate broadband tunable coupling while maintaining an ultra-high Q in 10-meter-coil and 4-meter-coil resonators at NIR wavelengths and in a ring resonator at visible wavelengths (698 nm and 780 nm). In the NIR coil resonators, this approach enables broadband critical coupling from 1550 to 1630 nm in a 10-meter-coil resonator. Tunable two-point coupling in the visible ring resonator enables critical coupling or close to critical coupling for a TM resonance at 698 nm and a TE resonance at 780 nm, while maintaining a 0.83 dB/m loss

at 698 nm and 1.20 dB/m loss at 780 nm. The two-point-coupled 10-meter-coil resonator can tune its coupling and be critically coupled from 1550 nm to 1630 nm while maintaining ultra-high intrinsic Q and low waveguide loss. The 10-meter-coil resonator measures a 340-million intrinsic Q at 1570 nm, demonstrating that the two-point-coupling design does not create excess loss, allowing us to reach the regime greater than 100-million intrinsic Q. Using the two-point-coupled 10-meter-coil resonator as an optical reference, we stabilize a laser at multiple critically coupled wavelengths from 1550 to 1630 nm, achieving a frequency noise reduction of six orders of magnitude and an integral linewidth of 334 Hz at all these wavelengths (1554 nm, 1585 nm, and 1600 nm). We also demonstrate that this design can be used to characterize waveguide loss in a large wavelength window for a specific waveguide mode (fundamental TE mode). By tuning a 4-meter-coil resonator coupling to near zero, the waveguide intrinsic loss is measured from 1250 nm to 1650 nm, revealing the O-H absorption peak at 1385 nm and N-H absorption peak at 1520 nm with the minimum loss of 0.14 dB/m near 1580 nm, corresponding to a 185-million intrinsic Q. Based on this waveguide loss spectrum measurement, we use secondary ion mass spectroscopy (SIMS) to determine that hydrogen impurities reside primarily in the silicon nitride layer with an atomic concentration of $\sim 6 \times 10^{19}$ atoms/cm^3, providing a path to further loss reduction through improved fabrication processes. The novelty of this work is the demonstrations of employing the two-point-coupling approach, showing that it can achieve excellent coupling versatility in photonic integrated waveguide resonators to achieve different coupling regimes, and proper coupling for drastically different wavelengths and waveguide modes such as TE and TM. These results can greatly benefit a wide range of optical and quantum applications, such as quantum computing and sensing, fiber sensing, optical atomic clocks, precision metrology, and low-noise microwave generation.

2. TWO-POINT-COUPLING DESIGN AND RESULTS

A. Two-Point-Coupled NIR Coil Resonator

Tunable two-point coupling, which is an unbalanced MZI as illustrated in Fig. 1, can achieve resonator coupling tuning by changing the phase section (ϕ) between zero coupling and its maximum coupling, $\kappa^2_{\max} = 4\kappa_0^2(1-\kappa_0^2)$, determined by its single coupler coupling coefficient κ_0^2 [45], and the tunable two-point coupling can be expressed as $\kappa^2 = \kappa^2_{\max}\cos^2(\phi/2)$ and the coupling rate for a bus-coupled waveguide resonator can be expressed as $\gamma_c = c\log[1/(1-\kappa^2)]/n_g L$, which is approximated to $\gamma_c = c\kappa^2/n_g L$ when $\kappa^2 \ll 1$ [49–51]. The maximum coupling $\kappa^2_{\max}$ needs to be sufficiently large to provide a wide tuning range. In this work, we employ both probe laser wavelength tuning and local temperature tuning using an on-chip micro-metal heater to demonstrate coupling tunability. In wavelength tuning, the tuning period is directly related to the MZI delay (δL) and corresponds to the MZI free spectral range (FSR), that is, $\delta\lambda_{2\pi} = \lambda^2/n_g L$. Similarly, for temperature tuning, a longer MZI delay leads to a shorter temperature tuning period.

In this work, we realized both a 10-meter-coil resonator and a 4-meter-coil resonator with two-point-coupling designs that enable the resonator to be critically coupled over a wide wavelength range in the NIR. The 6-μm-wide by 80-nm-thick silicon nitride waveguide design using the fundamental TE mode (TE_0) results in a small critical bending radius below 1 mm and a small modal crosstalk and coupling between the TE_0 and TE_1 modes (see Appendix A for the bending loss and S-bend modal crosstalk simulations) while maintaining an intrinsic waveguide loss below 0.1 dB/m at the C- and L-band wavelengths, so that the 10-meter-coil resonator can have a small footprint (~1 square inch). For both the NIR 10-meter-coil and 4-meter-coil resonator designs, the two-point coupler has a 0.28-mm-long phase delay section that corresponds to $\delta\lambda_{2\pi} = 5.6$ nm at 1550 nm and two identical directional couplers, while the directional coupler in the 10-meter-coil resonator has a 2.5-μm gap and 1.4-mm coupling length and that in the 4-meter-coil resonator has a 2.5-μm gap and 1.0 mm coupling length. Both the 10-meter-coil and 4-meter-coil resonators are designed in the fashion illustrated in Fig. 1(a). In the directional coupler design, the first S-bend in the bus waveguide brings the bus waveguide close to the resonator waveguide with the

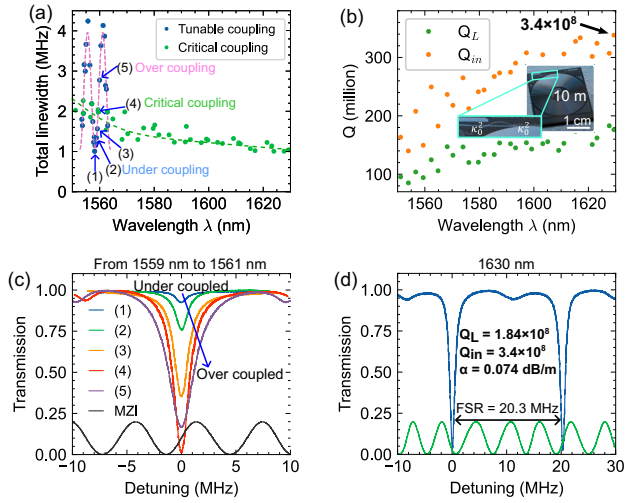

Fig. 2. Two-point-coupled 10-meter-coil resonator with 340-million intrinsic Q. (a) The measured resonator linewidth from 1550 nm to 1630 nm shows resonator coupling tuning with respect to wavelength with a tuning period of 5.6 nm, where critical coupling can be found across the wavelength range from 1550 nm to 1630 nm. The purple dashed line is a sinusoidal function fitted to the blue-dot data points based on the tunable coupling model by $\kappa^2 = 4\kappa_0^2(1-\kappa_0^2)\cos^2(\phi/2)$, and the green dashed line is merely a trend line interpolated from the green-dot data points. (b) The loaded and intrinsic Q of the critically coupled resonances show an intrinsic Q of 200 million at approximately 1550 nm and 340 million at 1630 nm. Inset shows a picture of the 10-meter-coil resonator and a zoomed-in view of the two-point coupler section. (c) The resonance gradually changes from being under-coupled to critically coupled and over-coupled from 1558.6 nm to 1561.3 nm corresponding to data points labeled as (1)–(5). (d) The spectral scan of the critically coupled resonance at 1630 nm measures a loaded Q of 184 million and an intrinsic Q of 340 million, corresponding to a waveguide propagation loss of 0.074 dB/m.

2.5-μm gap followed by a straight waveguide coupling section of either 1.0 mm or 1.4 mm, and the second S-bend takes the bus waveguide to exit the coupling section, as illustrated in Fig. 1(a). The bus waveguide in both the 10-meter-coil and 4-meter-coil resonators is tapered to 1.5 μm wide to maximize the waveguide-to-fiber edge coupling efficiency (see Appendix A for the edge coupling simulation). The 10-meter-coil resonators have a larger optical mode volume and a lower TRN limit in laser stabilization applications than the 4-meter-coil ones [19,28,29], while the 4-meter-coil resonators have a larger FSR of ∼50 MHz and this 50-MHz resonance spectral separation avoids the modal overlapping between adjacent resonances and makes the measurements of resonator linewidth and waveguide loss more reliable.

To characterize the tunable coupling and intrinsic resonator loss of the 10-meter-coil resonator, a spectral scan using a tunable laser and a fiber MZI with a 5.87-MHz FSR resolves the varying resonator linewidth and loaded Q as the resonator coupling is tuned with respect to the wavelength [Fig. 2(a)]. The two-point coupling is measured to have a maximum that is four times the waveguide intrinsic loss with a tuning period of ∼5.6 nm around 1550 nm. From 1559 nm to 1561 nm, while tuning the coupling from under- through critically to over-coupled, the coil resonator can be critically coupled twice within each tuning period. Therefore, the coil resonator is critically coupled approximately every ∼2.8 nm from 1550 nm to 1630 nm [Fig. 2(a)]. Figure 2(b) shows the measured loaded and intrinsic Q of the critically coupled resonances from 1550 nm to 1630 nm, which measures 340-million intrinsic Q and an equivalent waveguide loss of 0.074 dB/m at 1630 nm [Fig. 2(d)]. To investigate whether the two-point coupling design in this greater-than-100-million intrinsic Q regime adds excess loss to the resonator [47], a single-point-coupled 10-meter-coil resonator is designed, fabricated, and tested, with the design parameters except the coupling design identical to those in the two-point-coupled 10-meter-coil resonator. The measured waveguide loss and intrinsic Q in the single-point-coupled and two-point-coupled coil resonators match well (see Appendix B), indicating that the conventional two-point coupling does not create excess loss. The critical coupling wavelength range in the single-point-coupled coil resonator is ∼30 nm, ranging from 1580 nm to 1610 nm (see Appendix B), which is consistent with other recent studies on ultra-high-Q silicon nitride waveguide resonators [10,13]. In contrast, the two-point coupling design achieves a critical coupling wavelength range of up to 80 nm while maintaining the ultra-low propagation loss.

B. Two-Point-Coupled Visible Ring Resonator with *in-situ* Thermal Tuning

Ultra-high-Q silicon nitride ring resonators at visible wavelengths have demonstrated narrow linewidth Brillouin lasers [27] and laser stabilization for atomic spectroscopy applications [52]. Because resonator critical coupling at specific wavelengths for Sr or Rb atom experiments, such as 698 nm and 780 nm, is needed, we need to employ an *in-situ* tuning approach, such as thermal tuning, to tune the two-point coupling at one wavelength. We designed an ultra-high-Q ring resonator for 698 nm and 780 nm with a 3.79-mm radius and a 2.5-μm-wide by

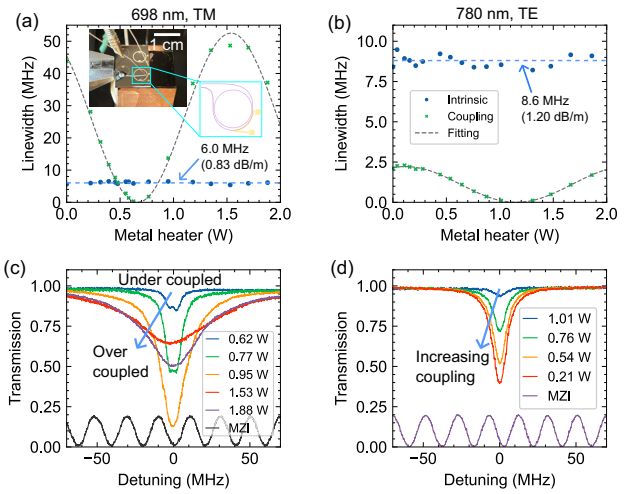

Fig. 3. Tunable two-point-coupled visible resonator with *in-situ* thermal tuning of two-point coupling. (a) Measurements of the resonator intrinsic and coupling linewidths for the TM_0 mode at 698 nm show that the thermal tuning of the two-point coupling tunes the resonator coupling while the resonator intrinsic loss stays constant and the waveguide loss is measured to be 0.83 dB/m, corresponding to a 71-million intrinsic Q. Inset shows a picture of the visible-wavelength ring resonator device on the testing stage with a zoomed-in illustration of the thermally tuned two-point coupling section. (b) Measured resonator intrinsic and coupling linewidths for the TE_0 mode at 780 nm while thermally tuning the two-point coupling show the two-point coupling tuning and a waveguide loss of 1.20 dB/m, corresponding to a 44-million intrinsic Q. (c) When thermally increasing the two-point coupling, the 698-nm TM resonance translates from being under-coupled to critically coupled and over-coupled. (d) Tuning the two-point coupling changes the 780-nm TE resonance coupling from weak coupling to under-coupling.

40-nm-thick silicon nitride waveguide design that supports both TE_0 and TM_0 modes at both 698 nm and 780 nm. A two-point coupling with two identical point couplers with a coupling gap of 2.2 μm, a 12.0-mm-long phase tuning section, and 0.5-mm-long unbalanced differential length is designed for the ring resonator, as shown by the insets in Fig. 3(a). In the thermal tuning of one arm of the unbalanced MZI of the two-point coupler, the absolute tuning arm length L determines the thermal tuning strength, as expressed by $\delta\phi = \frac{2\pi L}{\lambda}\frac{\partial n}{\partial T}\delta T$, while the unbalanced differential length ΔL determines the phase tuning strength by changing the input light wavelength, as expressed by $\delta\phi = \frac{2\pi n_g \Delta L \delta\lambda}{\lambda^2}$. Therefore, it is important to design a long MZI arm length for the two-point coupler covered by the microheater to achieve stronger thermal tuning. A 250-nm-thick, 80-μm-wide, and 8.15-mm-long Pt metal heater is deposited on top of the two-point coupler waveguide covering half of the phase tuning section, resulting in an effective 6.0-mm-long thermally tuned phase section, as shown by the insets in Fig. 3(a), and the resistance of the metal heater is calculated to be 43 Ω and measured to be 44 Ω. Therefore, at 698 nm, the effective 6.0-mm-long phase tuning section requires temperature tuning by the metal heater of ∼12 K to cover a full 2π phase tuning, while the 0.5-mm differential

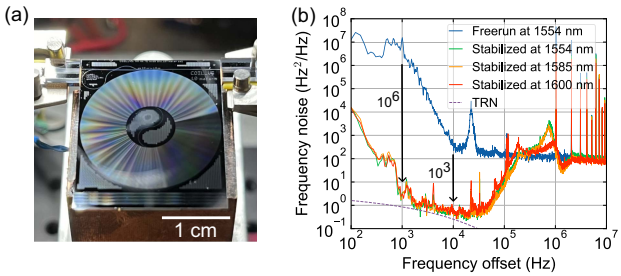

Fig. 4. Laser stabilization and frequency noise reduction at multiple wavelengths in the C and L bands using a two-point-coupled 10-meter-coil resonator with a 340-million intrinsic Q. (a) Photograph of the 10-meter-coil resonator. (b) At 1554 nm, 1585 nm, and 1600 nm, the 10-meter-coil resonator is critically coupled and used for laser stabilization, which shows frequency reduction of six orders of magnitude at 1 kHz offset and three orders of magnitude at 10 kHz offset.

arm length requires the input laser wavelength tuning of 0.65 nm.

By thermally heating the two-point coupling phase section, the TM_0 resonance at 689 nm experiences under-coupling, critical coupling, and over-coupling, as the maximum coupling is ~10 times higher than the ring resonator intrinsic loss [Figs. 3(a) and 3(c)]. The maximum coupling for the TE_0 mode at 780 nm is much lower, as the TE_0 mode is more confined than the TE_0 mode; thus, the resonator can be tuned from being weakly coupled to under-coupled [Figs. 3(b) and 3(d)]. While the coupling is being thermally tuned, the resonator intrinsic loss stays constant at around 0.83 dB/m at 698 nm and 1.20 dB/m at 780 nm [Figs. 4(b) and 4(d)]. For both 698 nm and 780 nm, the full tuning period in the thermal heating power is measured to be ~0.85 W, meaning that 0.85 W heating power corresponds to the previously estimated temperature change of 12 K and the thermal impedance is inferred to be 14.1 K/W. The TM_0 mode at 698 nm and TE_0 mode at 780 nm can be critically coupled or nearly critically coupled, while the TE_0 mode at 698 nm and TM_0 mode at 780 nm are outside the coupling reach and their resonances are not observed.

C. Laser Stabilization at Multiple Critically Coupled Wavelengths

The ability to tune the resonator coupling to critical coupling for an integrated bus-coupling waveguide reference maximizes the SNR of frequency noise discrimination and noise suppression in the PDH lock [30]. The two-point-coupled 10-meter-coil resonator is critically coupled every ~2.8 nm while maintaining 200-million intrinsic Q from 1550 nm to 1630 nm and is used to demonstrate laser stabilization. A widely tunable laser (Velocity TLB-6700) is used to probe the coil reference resonator and demonstrate the PDH lock at multiple critically coupled wavelengths, 1554 nm, 1585 nm, and 1600 nm, where the free-running and stabilized laser frequency noise are measured with a 1.026-MHz FSR unbalanced fiber MZI [19,53]. The PDH lock bandwidth reaches ~1 MHz and suppresses the laser frequency noise by six orders of magnitude at 1-kHz offset and three orders of magnitude at 10 kHz, reducing the integral linewidth to 334 Hz from the 22-kHz free-running integral linewidth (Fig. 4). The laser stabilization performances at three different wavelengths are nearly identical, and the stabilized laser frequency noise reaches the TRN from 1-kHz to 40-kHz offset, indicating sufficiently large SNRs in frequency noise discrimination. The measured 334-Hz integral linewidth is limited by the fiber noise in the unbalanced MZI used for measuring the laser frequency noise and is expected to be much lower when measured using the heterodyne beatnote technique with an ultra-stable laser [19].

D. Waveguide Loss Spectrum and Secondary Ion Mass Spectroscopy

We demonstrate that by tuning the coupling to near zero over a large wavelength range without adding excess loss to the resonator, we can accurately measure the waveguide intrinsic loss and Q over a wide wavelength range [46]. For this measurement, we used a two-point-coupled 4-meter-coil resonator while all design aspects are the same as the 10-meter-coil resonator except for a smaller S-bend radius of 1.1 mm. The waveguide loss is measured every ~5.6 nm at the weakly coupled resonances, which reaches near zero every ~5.6 nm [Fig. 5(a)]. The measurement of the intrinsic linewidth and waveguide loss using weakly coupled resonances compared to critically coupled resonances is more robust and less sensitive to the resonance extinction ratio degradation due to stray light or polarization misalignment between the fiber mode and waveguide fundamental TE mode (see the uncertainty sensitivity analysis in Appendix B). When such tuning on resonator coupling is not available and the intrinsic linewidth measurement over a wide wavelength range goes through different coupling regimes, which is still the predominant approach for measuring ultra-low waveguide losses reported in the literature [10,12,13], eliminating the sources of resonance extinction degradation in experiments is critical to the accuracy and reliability of the resonator intrinsic linewidth and waveguide loss.

The waveguide loss spectrum shows two absorption loss peaks near 1385 nm and 1520 nm, which are related to O-H and N-H absorption, respectively [54,55]. Outside the O-H and N-H absorption loss dominated wavelength regions, the loss is primarily due to scattering loss, as the $1/\lambda^4$ scattering loss model fits well with the loss spectrum outside the absorption loss peaks [Fig. 4(a)]. A recent study of the broadband loss spectrum of a high-Q etched silica resonator shows the O-H absorption peak of 0.15 dB/m at 1385 nm and estimates the O-H content level to be 2.4 ppm in silica [40]. Loss measurements on high-Q silicon nitride waveguide resonators in the ultra-low-loss (below 1 dB/m) regime from 1460 nm to 1630 nm also show a N-H absorption peak near 1520 nm [13]. These combined results [Fig. 5(a)] indicate that further reduction of hydrogen impurities will be critical even in the state-of-the-art ultra-low-loss silicon nitride waveguide fabrication processes [10,12,13]. The increased waveguide loss in the 4-meter-coil resonator compared to the 10-meter-coil one is likely due to a smaller S bend (see Appendix A).

To determine where the hydrogen impurity resides near the silicon nitride waveguide layer, we use a 4-meter-coil resonator chip for a secondary ion mass spectroscopy (SIMS) measurement to sample the hydrogen concentration at different depths [Fig. 5(b)]. The bottom cladding oxide is a 15-μm

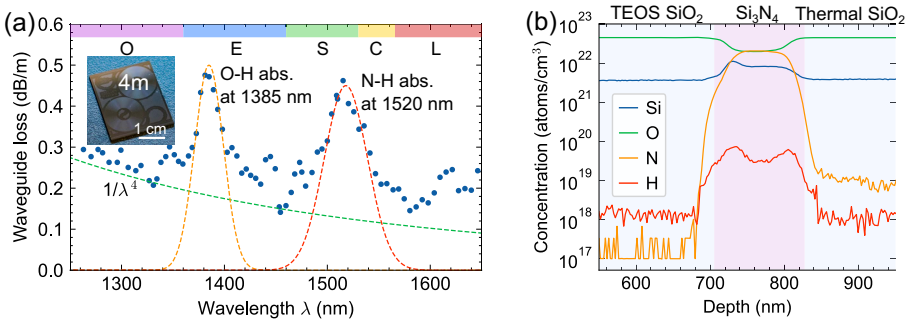

Fig. 5. (a) Silicon nitride waveguide loss spectrum measured in the two-point-coupled 4-meter-coil waveguide resonator shows the absorption loss peaks near 1385 nm and 1520 nm related to hydrogen impurities. (b) SIMS depth profiling measures the hydrogen impurity level at different depths and layers, revealing ~6×10^{19} atoms/cm^3 hydrogen impurity level in the silicon nitride layer. The SIMS spot is on a 2 mm by 2 mm area of the fill pattern with 50% nitride and 50% TEOS oxide upper cladding.

thermally grown oxide. An 80-nm silicon nitride layer is deposited by low-pressure chemical vapor deposition (LPCVD). The 6-μm silicon dioxide upper cladding is deposited by plasma-enhanced chemical vapor deposition with tetraethoxysilane (TEOS-PECVD) as a precursor and chemically etched away to 700 nm for the SIMS measurement. The SIMS measurement reveals that the hydrogen impurities show up in the LPCVD silicon nitride layer with an atomic concentration of ~6×10^{19} atoms/cm^3. Note that the SIMS data in the silicon nitride layer [pink region in Fig. 5(b)] contain oxygen because the measurement is on a 50% fill pattern area where there is half LPCVD nitride and half TEOS oxide. The hydrogen content in the nitride layer can be twice the measured value in Fig. 5(b), ~1.2×10^{21} atoms/cm^3. The SIMS detection limit for hydrogen in silicon dioxide is typically 1×10^{18} atoms/cm^3 [56]. Both the LPCVD silicon nitride deposition and TEOS-PECVD oxide deposition processes involve a large amount of hydrogen, whereas the thermal oxide growth does not involve hydrogen. The SIMS measurement leads to two important observations: first, the hydrogen content mainly resides in the LPCVD nitride layer and can be further reduced by adding annealing steps; second, although the TEOS-PECVD oxide deposition involves hydrogen, the TEOS-PECVD oxide is as good as the thermal oxide at the 1×10^{18} atoms/cm^3 SIMS detection limit for hydrogen.

3. DISCUSSION AND CONCLUSION

We have demonstrated for the first time a two-point-coupled ultra-high-Q 10-meter-coil silicon nitride waveguide resonator that is critically coupled every ~2.8 nm from 1550 nm to 1630 nm and measures a 340-million intrinsic Q and 0.074-dB/m waveguide propagation loss. We also validate that the two-point-coupling design does not create excess loss in the ultra-high-Q regime. A visible and NIR silicon nitride ring resonator with two-point coupling and *in-situ* thermal tuning achieves critical coupling for the TM_0 mode at 698 nm and near critical coupling for the TE_0 mode at 780 nm in a single resonator, where during the thermal tuning on the two-point coupler the waveguide loss is measured to maintain 0.83 dB/m at 698 nm and 1.20 dB/m at 780 nm. Using the two-point-coupled 10-meter-coil resonator as an optical reference, we stabilize a laser with a frequency noise reduction of six orders of magnitude at multiple critically coupled wavelengths from 1550 nm to 1630 nm.

There is a tradeoff in designing the two-point coupler's differential MZI length and using the wavelength tuning or device-global temperature tuning that a longer unbalanced length makes it easier to tune the coupling by wavelength but can also increase its sensitivity to environmental temperature changes. The NIR 10-meter-coil and 4-meter-coil resonators have a 0.28-mm phase tuning section that requires a device-global temperature increase of up to 500 K to achieve complete π phase tuning, which makes it robust to environmental temperature changes but can only rely on input light wavelength tuning for coupling tuning. However, *in-situ* thermal tuning on one MZI arm relies on the absolute length of the tuning arm, but not on the differential arm length, and it is not subject to the tradeoff mentioned above. Thus, the *in-situ* thermal tuning can be more advantageous in that the two-point coupler can have strong tuning strength owing to a long absolute thermal tuning length, and a small differential arm length makes the tuning insensitive to the input light wavelength or device temperature changes. However, these micro thermal heaters consume a considerable amount of power during tuning. Fully planar and wafer-scale integration of piezoelectric (PZT, lead zirconate titanate) actuators that provide strong and fast waveguide index tuning with very low power consumption [57] with a two-point coupling design can potentially enable new applications, such as fast Q-switching in integrated ultra-high-Q waveguide resonators. The capability of resonator coupling tuning can also benefit quantum photonics applications, such as photon-pair generation based on spontaneous OPO processes, by making a high-extinction optical filter for filtering out the strong pump light in photon-pair generation by fine-tuning the resonator coupling to reach critical coupling as closely as possible.

We also demonstrate that two-point coupling enables the measurement of waveguide loss mechanisms in a large wavelength window for a specific waveguide mode (fundamental TE mode) by tuning the coupling loss to near zero and measuring the under-coupled resonances. The waveguide intrinsic loss measured from a two-point-coupled 4-meter-coil resonator

from 1250 nm to 1650 nm shows the absorption peaks at 1385 nm and 1520 nm, which are related to hydrogen impurities. The SIMS measurement on the 4-meter-coil resonator reveals that hydrogen impurities reside primarily in the LPCVD silicon nitride layer with an atomic concentration of $\sim 6 \times 10^{19}$ atoms/cm^3, indicating that reducing the hydrogen content in the LPCVD silicon nitride can further decrease the silicon nitride waveguide propagation loss in the sub-0.1-dB/m loss regime, making it possible to achieve all waveguide resonators with a billion Q factor. These results demonstrate the capability of critically coupling the resonator over a wide wavelength window, tuning the resonator coupling with *in-situ* actuators, and proper coupling for different waveguide modes and wavelengths. This can enhance the performance of applications, such as self-injection locked lasers, laser stabilization, squeezed light generation, and efficient OPO emitters, and greatly benefit AMO experiments and applications, quantum computing and sensing, fiber sensing, optical atomic clocks, precision metrology, and low-noise microwave generation.

APPENDIX A: COIL RESONATOR DESIGN CONSIDERATION

The 10-meter-coil waveguide resonator [Fig. 6(a)] design considerations include waveguide-bending-related properties such as bending loss, S-bend point loss, and mode conversion due to the bending mode mismatch and bus waveguide taper design to optimize the chip-to-fiber edge coupling efficiency. A bend loss simulation using Lumerical MODE for the 6-μm and 80-nm silicon nitride waveguides at 1550 nm shows that the critical bending radius for the TE_0 mode is below 1.0 mm [Fig. 6(b)]. The S-bend point loss [Fig. 6(c)] and mode conversion [Fig. 6(d)] between the waveguide modes especially between the TE_0 and TE_1 modes suggest the S-bend radius needs

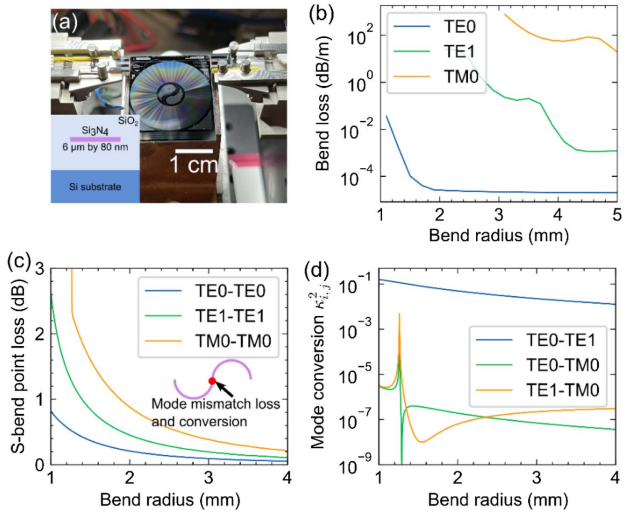

Fig. 6. Bending loss, S-bend point loss, S-bend mode conversion simulation in 6-μm and 80-nm silicon nitride waveguides at 1550 nm. (a) The TE_0 mode has negligible bending loss at bending radii above 1.0 mm. (b) The TE_0 mode has a 0.2–0.8 dB point loss at the S-bend center with a bend radius from 1 mm to 2 mm. (c) Mode conversion between the TE_0 and TE_1 modes due to mode mismatches where the S-bending direction turns in the opposite direction.

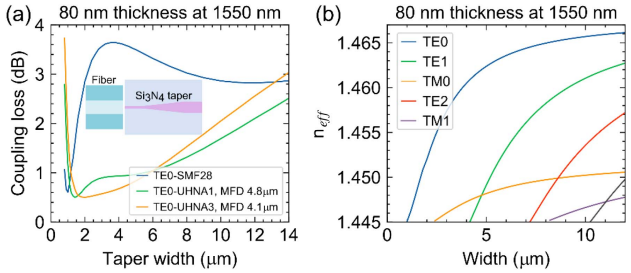

Fig. 7. Waveguide taper design for edge coupling. (a) Coupling loss between TE_0 and three types of fibers with different mode field diameters (MFDs)—SMF28, UHNA1, and UHNA3—shows that a 1.5-μm taper can achieve coupling loss below 1.0 dB. (b) Waveguide effective index (n_{eff}) simulation shows that the tapered waveguide is single mode below 2.2 μm in taper width.

to be 2.0 mm or above to minimize the unwanted TE_0-TE mode coupling and conversion. The bus waveguide is tapered to 1.5 μm at the edge coupling with different types of fibers, such as standard single-mode fibers (SMF28) and ultra-high-numerical-aperture fibers (UHNA), to reduce the coupling loss to less than 1.0 dB per facet [Fig. 7(a)] and to create a single-mode tapered waveguide that only efficiently couples the TE_0 mode [Fig. 7(b)].

APPENDIX B: LOSS COMPARISON BETWEEN ONE- AND TWO-POINT-COUPLED RESONATORS

The linewidth, loss, and Q of a one-point-coupled 10-meter-coil resonator are measured from 1550 nm to 1630 nm for comparison with the two-point-coupled 10-meteer-coil resonator, as shown in Fig. 8. The one-point-coupled coil resonator exhibits a critical coupling wavelength range of ~30 nm from 1580 nm to 1610 nm, and the waveguide loss measurement in Fig. 8(b) in both resonators shows that the two-point coupling does not create additional coupler losses.

The fitting used in the waveguide resonator linewidth and loss measurements is based on the add-through transmission

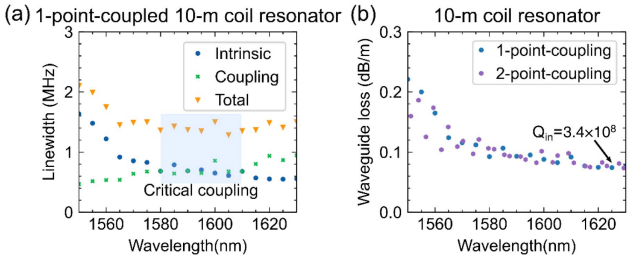

Fig. 8. Measured intrinsic resonator waveguide loss comparison between one-point-coupled and two-point-coupled 10-meter-coil silicon nitride waveguide resonators. (a) The measured intrinsic, coupling, and total resonator linewidths in a one-point-coupled 10-meter-coil resonator show the critical coupling wavelength region from 1580 nm to 1610 nm. (b) The measured waveguide loss in both the one-point-coupled and two-point-coupled 10-meter-coil resonators shows almost identical loss spectra.

that is a function of both the intrinsic (γ_{in}) and external (γ_{ex}) coupling linewidths, expressed as $T = |\frac{i\Delta\omega+(\gamma_{in}-\gamma_{ex})^2/4}{i\Delta\omega+(\gamma_{in}+\gamma_{ex})^2/4}|^2$, where the transmission minimum related to the extinction ratio can be found as $T_{min} = |\frac{\gamma_{in}-\gamma_{ex}}{\gamma_{in}+\gamma_{ex}}|^2$. Clearly, the resonance reaches the maximum extinction ratio when $T_{min} = 0$ at critical coupling. If we constrain our analysis to the under-coupled regime of $\gamma_{in} \geq \gamma_{ex}$, the intrinsic linewidth can be expressed in terms of T_{min} and $\Delta\omega_{FWHM} = \gamma_{in} + \gamma_{ex}$ by $\gamma_{in} = \Delta\omega_{FWHM}(1 + \sqrt{T_{min}})/2$. This equation informs us how sensitive to the uncertainty in the extinction ratio the intrinsic linewidth measurement is, as inevitably there could be stray light or a small misalignment between the fiber polarization and the bus waveguide fundamental TE mode that is the targeted resonance waveguide mode to be measured, any of which introduces degradation of the resonance extinction or increasement in T_{min}. At critical coupling, the intrinsic loss measurement is most sensitive to the extinction ratio uncertainty, while it becomes less sensitive as the resonance is more weakly coupled and T_{min} is closer to one. For instance, degradation of T_{min} by 1% at critical coupling and $T_{min} = 0$ causes a measurement uncertainty of 10% in γ_{in}, while it only causes a measurement uncertainty of 0.4% at $T_{min} = 0.5$ (γ_{in}:$\gamma_{ex} = 5.8$:1) and 0.3% at $T_{min} = 0.8$ (γ_{in}:$\gamma_{ex} = 18$:1). Therefore, with such experimental uncertainties, the intrinsic loss measurement using under-coupled resonances is more reliable.

Funding. DARPA Microsystems Technology Office (HR0011-22-2-0008); Army Research Office (W911NF-23-1-0179).

Acknowledgment. We thank Shuman Sun and Yi Xu at University of Virginia for the use of the Santac O-band tunable laser and Mohamad Hossein Idjadi and Nicolas K. Fontaine at Nokia Bell Labs for the use of the Santac widely tunable laser. The views and conclusions contained in this document are those of the authors and should not be interpreted as representing the official policies of DARPA or the U.S. government.

Disclosures. The authors declare no conflicts of interest.

Data Availability. Data underlying the results presented in this paper are not publicly available at this time but may be obtained from the authors upon reasonable request.

REFERENCES

1. A. Orieux and E. Diamanti, "Recent advances on integrated quantum communications," J. Opt. **18**, 083002 (2016).
2. H. Yonezawa, D. Nakane, T. A. Wheatley, *et al.*, "Quantum-enhanced optical-phase tracking," Science **337**, 1514–1517 (2012).
3. G. Zhang, J. Y. Haw, H. Cai, *et al.*, "An integrated silicon photonic chip platform for continuous-variable quantum key distribution," Nat. Photonics **13**, 839–842 (2019).
4. D. G. Matei, T. Legero, S. Häfner, *et al.*, "1.5 μm lasers with sub-10 mHz linewidth," Phys. Rev. Lett. **118**, 263202 (2017).
5. A. D. Ludlow, M. M. Boyd, J. Ye, *et al.*, "Optical atomic clocks," Rev. Mod. Phys. **87**, 637–701 (2015).
6. J. Li, H. Lee, and K. J. Vahala, "Microwave synthesizer using an on-chip Brillouin oscillator," Nat. Commun. **4**, 2097 (2013).
7. S. Sun, B. Wang, K. Liu, *et al.*, "Integrated optical frequency division for microwave and mmWave generation," Nature **627**, 540–545 (2024).
8. I. Kudelin, W. Groman, Q.-X. Ji, *et al.*, "Photonic chip-based low-noise microwave oscillator," Nature **627**, 534–539 (2024).
9. D. J. Blumenthal, R. Heideman, D. Geuzebroek, *et al.*, "Silicon nitride in silicon photonics," Proc. IEEE **106**, 2209–2231 (2018).
10. M. W. Puckett, K. Liu, N. Chauhan, *et al.*, "422 Million intrinsic quality factor planar integrated all-waveguide resonator with sub-MHz linewidth," Nat. Commun. **12**, 934 (2021).
11. K. Liu, N. Jin, H. Cheng, *et al.*, "Ultralow 0.034 dB/m loss wafer-scale integrated photonics realizing 720 million *Q* and 380 μW threshold Brillouin lasing," Opt. Lett. **47**, 1855–1858 (2022).
12. W. Jin, Q.-F. Yang, L. Chang, *et al.*, "Hertz-linewidth semiconductor lasers using CMOS-ready ultra-high-*Q* microresonators," Nat. Photonics **15**, 346–353 (2021).
13. C. Xiang, W. Jin, O. Terra, *et al.*, "3D integration enables ultralow-noise isolator-free lasers in silicon photonics," Nature **620**, 78–85 (2023).
14. N. Chauhan, J. Wang, D. Bose, *et al.*, "Ultra-low loss visible light waveguides for integrated atomic, molecular, and quantum photonics," Opt. Express **30**, 6960–6969 (2022).
15. Y. Fan, A. van Rees, P. J. M. van der Slot, *et al.*, "Hybrid integrated InP-Si_3N_4 diode laser with a 40-Hz intrinsic linewidth," Opt. Express **28**, 21713–21728 (2020).
16. S. Gundavarapu, G. M. Brodnik, M. Puckett, *et al.*, "Sub-hertz fundamental linewidth photonic integrated Brillouin laser," Nat. Photonics **13**, 60–67 (2018).
17. K. Liu, J. Wang, M. Harrington, *et al.*, "Integrated photonic molecule Brillouin laser with high power sub-100-mHz fundamental linewidth," Opt. Lett. **49**, 45–48 (2023).
18. T. Kessler, C. Hagemann, C. Grebing, *et al.*, "A sub-40-mHz-linewidth laser based on a silicon single-crystal optical cavity," Nat. Photonics **6**, 687–692 (2012).
19. K. Liu, N. Chauhan, J. Wang, *et al.*, "36 Hz integral linewidth laser based on a photonic integrated 4.0 m coil resonator," Optica **9**, 770–775 (2022).
20. N. Chauhan, C. Caron, J. Wang, *et al.*, "Trapped ion qubit and clock operations with a visible wavelength photonic coil resonator stabilized integrated Brillouin laser," arXiv, arXiv:2402.16742 (2024).
21. R. J. Niffenegger, J. Stuart, C. Sorace-Agaskar, *et al.*, "Integrated multi-wavelength control of an ion qubit," Nature **586**, 538–542 (2020).
22. J. L. Bohn, A. M. Rey, and J. Ye, "Cold molecules: progress in quantum engineering of chemistry and quantum matter," Science **357**, 1002–1010 (2017).
23. W. Bogaerts, P. D. Heyn, T. V. Vaerenbergh, *et al.*, "Silicon microring resonators," Laser Photon. Rev. **6**, 47–73 (2012).
24. H. Lee, T. Chen, J. Li, *et al.*, "Chemically etched ultrahigh-*Q* wedge-resonator on a silicon chip," Nat. Photonics **6**, 369–373 (2012).
25. K. Y. Yang, D. Y. Oh, S. H. Lee, *et al.*, "Bridging ultrahigh-*Q* devices and photonic circuits," Nat. Photonics **12**, 297–302 (2018).
26. Z. Yuan, H. Wang, L. Wu, *et al.*, "Linewidth enhancement factor in a microcavity Brillouin laser," Optica **7**, 1150–1153 (2020).
27. N. Chauhan, A. Isichenko, K. Liu, *et al.*, "Visible light photonic integrated Brillouin laser," Nat. Commun. **12**, 4685 (2021).
28. G. Huang, E. Lucas, J. Liu, *et al.*, "Thermorefractive noise in silicon-nitride microresonators," Phys. Rev. A **99**, 061801 (2019).
29. H. Lee, M.-G. Suh, T. Chen, *et al.*, "Spiral resonators for on-chip laser frequency stabilization," Nat. Commun. **4**, 2468 (2013).
30. E. D. Black, "An introduction to Pound–Drever–Hall laser frequency stabilization," Am. J. Phys. **69**, 79–87 (2000).
31. C. A. López-Mercado, V. V. Spirin, J. L. B. Escobedo, *et al.*, "Locking of the DFB laser through fiber optic resonator on different coupling regimes," Opt. Commun. **359**, 195–199 (2016).
32. R. R. Galiev, N. M. Kondratiev, V. E. Lobanov, *et al.*, "Optimization of laser stabilization via self-injection locking to a whispering-gallery-mode microresonator," Phys. Rev. Appl. **14**, 014036 (2020).
33. A. Otterpohl, F. Sedlmeir, U. Vogl, *et al.*, "Squeezed vacuum states from a whispering gallery mode resonator," Optica **6**, 1375–1380 (2019).

34. Y. K. Chembo, "Quantum dynamics of Kerr optical frequency combs below and above threshold: spontaneous four-wave mixing, entanglement, and squeezed states of light," Phys. Rev. A **93**, 033820 (2016).
35. J. A. Black, G. Brodnik, H. Liu, *et al.*, "Optical-parametric oscillation in photonic-crystal ring resonators," Optica **9**, 1183–1189 (2022).
36. X. Lu, G. Moille, A. Singh, *et al.*, "Milliwatt-threshold visible–telecom optical parametric oscillation using silicon nanophotonics," Optica **6**, 1535–1541 (2019).
37. W. Weng, J. D. Anstie, T. M. Stace, *et al.*, "Nano-kelvin thermometry and temperature control: beyond the thermal noise limit," Phys. Rev. Lett. **112**, 160801 (2014).
38. B. Li, Z. Yuan, W. Jin, *et al.*, "High-coherence hybrid-integrated 780 nm source by self-injection-locked second-harmonic generation in a high-*Q* silicon-nitride resonator," Optica **10**, 1241–1244 (2023).
39. Q. Zhao, M. W. Harrington, A. Isichenko, *et al.*, "Integrated reference cavity with dual-mode optical thermometry for frequency correction," Optica **8**, 1481–1487 (2021).
40. L. Wu, M. Gao, J.-Y. Liu, *et al.*, "Hydroxyl ion absorption in on-chip high-*Q* resonators," Opt. Lett. **48**, 3511–3514 (2023).
41. H. Jayatilleka, H. Frish, R. Kumar, *et al.*, "Post-fabrication trimming of silicon photonic ring resonators at wafer-scale," J. Lightwave Technol. **39**, 5083–5088 (2021).
42. Y. Wu, H. Shang, X. Zheng, *et al.*, "Post-processing trimming of silicon photonic devices using femtosecond laser," Nanomaterials **13**, 1031 (2023).
43. P. Orlandi, F. Morichetti, M. J. Strain, *et al.*, "Tunable silicon photonics directional coupler driven by a transverse temperature gradient," Opt. Lett. **38**, 863–865 (2013).
44. M. J. Strain, C. Lacava, L. Meriggi, *et al.*, "Tunable *Q*-factor silicon microring resonators for ultra-low power parametric processes," Opt. Lett. **40**, 1274–1277 (2015).
45. X. Han, L. Wang, P. Zou, *et al.*, "A tunable optical waveguide ring resonator for microwave photonic filtering," in *IEEE International Topical Meeting on Microwave Photonics (MWP)* (IEEE, 2013), pp. 88–91.
46. H. Shoman, H. Jayatilleka, N. A. F. Jaeger, *et al.*, "Measuring on-chip waveguide losses using a single, two-point coupled microring resonator," Opt. Express **28**, 10225–10238 (2020).
47. D. T. Spencer, J. F. Bauters, M. J. R. Heck, *et al.*, "Integrated waveguide coupled Si_3N_4 resonators in the ultrahigh-*Q* regime," Optica **1**, 153–157 (2014).
48. J. Hinney, S. Kim, G. J. K. Flatt, *et al.*, "Efficient excitation and control of integrated photonic circuits with virtual critical coupling," Nat. Commun. **15**, 2741 (2024).
49. B. E. Little, S. T. Chu, H. A. Haus, *et al.*, "Microring resonator channel dropping filters," J. Lightwave Technol. **15**, 998–1005 (1997).
50. L. A. Coldren, S. W. Corzine, and M. L. Mashanovitch, *Diode Lasers and Photonic Integrated Circuits* (Wiley, 2012).
51. V. Van, *Optical Microring Resonators: Theory, Techniques, and Applications* (CRC Press, 2016).
52. A. Isichenko, N. Chauhan, J. Wang, *et al.*, "Tunable integrated 118 million *Q* reference cavity for 780 nm laser stabilization and rubidium spectroscopy," in *CLEO: Science and Innovations* (Optica Publishing Group, 2023), paper SF3K-4.
53. P. Horak and W. H. Loh, "On the delayed self-heterodyne interferometric technique for determining the linewidth of fiber lasers," Opt. Express **14**, 3923–3928 (2006).
54. J. F. Bauters, M. J. R. Heck, D. D. John, *et al.*, "Planar waveguides with less than 0.1 dB/m propagation loss fabricated with wafer bonding," Opt. Express **19**, 24090–24101 (2011).
55. W. Jin, D. D. John, J. F. Bauters, *et al.*, "Deuterated silicon dioxide for heterogeneous integration of ultra-low-loss waveguides," Opt. Lett. **45**, 3340–3343 (2020).
56. Z. Zhu, V. Shutthanandan, and M. Engelhard, "An investigation of hydrogen depth profiling using ToF-SIMS," Surf. Interface Anal. **44**, 232–237 (2012).
57. J. Wang, K. Liu, M. W. Harrington, *et al.*, "Silicon nitride stress-optic microresonator modulator for optical control applications," Opt. Express **30**, 31816–31827 (2022).